8-1-2021

Numerical performance of thermal conductivity in Bioconvection flow of cross nanofluid containing swimming microorganisms over a cylinder with melting phenomenon

Muhammad Imran
Government College University Faisalabad

Umar Farooq
Government College University Faisalabad

Hassan Waqas
Government College University Faisalabad

Ali E. Anqi
King Khalid University

Mohammad Reza Safaei
China Medical University Hospital

Case Studies in Thermal Engineering 26 (2021) 101181

Contents lists available at ScienceDirect

Case Studies in Thermal Engineering

journal homepage: www.elsevier.com/locate/csite

Numerical performance of thermal conductivity in Bioconvection flow of cross nanofluid containing swimming microorganisms over a cylinder with melting phenomenon

Muhammad Imran [a], Umar Farooq [a], Hassan Waqas [a], Ali E. Anqi [b], Mohammad Reza Safaei [c,d,e,*]

[a] Department of Mathematics, Government College University Faisalabad, 38000, Pakistan
[b] Department of Mechanical Engineering, College of Engineering, King Khalid University, Abha, 61421, Saudi Arabia
[c] Department of Medical Research, China Medical University Hospital, China Medical University, Taichung, Taiwan
[d] Mechanical Engineering Department, Faculty of Engineering, King Abdulaziz University, Jeddah, Saudi Arabia
[e] Department of Civil and Environmental Engineering, Florida International University, Miami, FL, USA

ARTICLE INFO

Keywords:
Cross nanofluid
Cylinder geometry
Non-linear thermal radiation
Shooting scheme
Bvp4c
Bioconvection
Motile microorganism

ABSTRACT

This study investigates the effects of melting phenomena and non-linear thermal radiation in Cross nanofluid bioconvection flow with motile microorganisms with a convective boundary over a cylinder. Brownian motion and thermophoresis diffusion are also taken into account in this mathematical model. A governing partial differential equation is used to represent the given flow phenomena. The proper dimensionless transformation is then employed to convert the PDE controlling system into an ordinary one. Bvp4c numerically solves redesigned ODE problems using a shooting strategy in the computational tool MATLAB. Figures versus velocity, temperature distribution, nanoparticle concentration, and microbe concentration profiles are used to analyze and expound on the notably involved aspects thoroughly. It has been demonstrated that increasing the estimates of a mixed convection parameter can enhance velocity. By increasing the Prandtl number, the temperature and concentration of nanoparticles decrease. A high Peclet value lowers the microorganism's profile.

1. Introduction

Heat convective liquids such as ethylene glycol, kerosene, water, and oil may be employed in various technical equipment [1]. These base fluids have limited thermal conductivity, or in other words, they have decreased thermal conductivity [2]. Nanofluids are made up of small nanoparticles and a base fluid [3]. As a result, the heat transformation characteristics of nano solid materials in conventional fluids have been enhanced [4]. Cooling systems, air conditioners, chillers, microelectronics, microchips in computer procedure, diesel engine oil, and fuel cells are only a few of the numerous prospective uses for nanofluids for heat transmission [5].

It should be noted that the thermal conductivity of nanofluids may be altered by adjusting the volume fraction, particle size, heat, and a few other factors [6]. Nanotechnology is essential in many sectors, including chemicals and metallurgical machinery, transportation, macroscopic products, cancer therapy, and power generation [7]. Choi [8] defined nanofluids as mixes of nanometer-sized

* Corresponding author. Department of Civil and Environmental Engineering, Florida International University, Miami, FL, USA.
E-mail addresses: msafaei@fiu.edu, cfd_safaei@yahoo.com (M.R. Safaei).

https://doi.org/10.1016/j.csite.2021.101181
Received 7 May 2021; Received in revised form 19 June 2021; Accepted 20 June 2021
Available online 24 June 2021

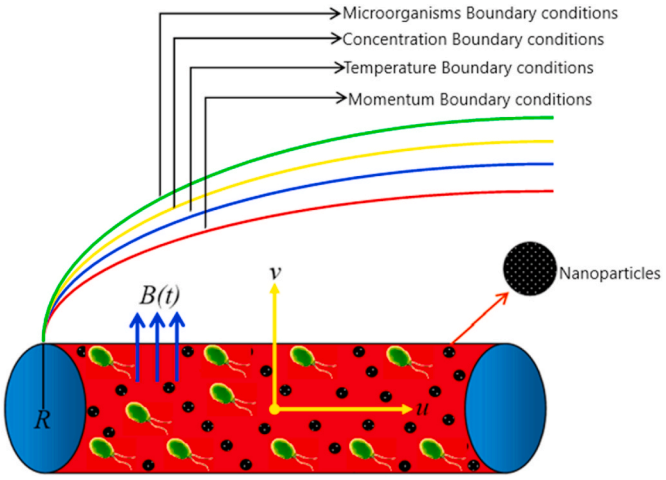

Fig. 1. Flow problem.

particle suspensions with standard fluids. Buongiorno [9] outlines two uncommon processes for increasing the standard convection rate of heat energy distribution: Brownian diffusion and thermophoresis motion effect. Venkatadri et al. [10] investigated the Melting heat exchange of an electrical conductor flow of nanofluid against an exponentially shrinking/expanding porous layer with a non-linear Radiative Cattaneo Christov heat flux in the presence of a magnetic field. Mondal et al. [11] investigated the effect of magnetohydrodynamic heat exchange on the flow of stagnation point nanoliquids across an extending or decreasing surface via homogeneous chemical processes. Radiative heat transfers of molten salt-based nanoliquids over cooling coils via non-uniform heat flow were explored by Ying et al. [12]. At the emergence of quadratic momentum, Zainal et al. [13] monitored the MHD hybrid nanofluid stream to the porous expanding/shrinking surface. Eid et al. [14] presented thermal conductivity change, including the effects of heat transfer on a magneto-water nanofluid moving in a porous channel with slippage. Numerous scholars are interested in studying nanofluids with the Buongiorno modal, as seen by references [15–22]. Kamal et al. [23] investigated analytically the properties of a viscoelastic copper nanofluid with a twofold diffusion problem caused by the 3-D flow of stagnation point induced by heat generation in a space environment. Anuar et al. [24] investigated Maxwell nanofluids' thermal radiative stagnation point moving over an inconsistent convectively warmed stretched surface. Rizwana et al. [25] examined the oblique stagnation point of a created magnet field flowing over an oscillating surface for a non-Newtonian liquid. Giri et al. [26] described the melting heat transfer mechanism in a Magnetohydrodynamic nanofluid flowing between two horizontally formed plates in a rotating configuration. Sharma et al. [27] examined the effects of variable thicknesses and melting of heat exchange on nanoliquids movement of Magnetohydrodynamic through the slender expanding surface.

The bioconvection process can be represented as germs swimming off in less dense substances than water. Because of the increased concentration of microorganisms, the upper layer of substances seems overly dense and frail, causing the microorganisms to break down owing to bioconvection movement. Gravitation (gravity acceleration), gyrotaxis, and oxytaxis (lower part-heavy) organisms are examples of such microorganisms. Microorganisms, some of which are the oldest organisms ever recognized to a human being, are crucial in various ways. Because of the up-swimming, microbe is identified as the development technique in microorganisms such as bacteria or algae. Bioconvection offers a wide range of applications in biochemistry and bioengineering. Biomedical engineering employs the bioconvection process in diesel fuel products, bioreactors, and fuel cell engineering. Platt [28] was the first to discover the phenomenon of bioconvection. Kuznetsov [29,30] may have been the first to use the term nanofluids bioconvection. Kuznetsov [31] expanded on this notion, concentrating on nanofluids and gyrotactic motile microorganisms, demonstrating that the consequent large-scale movement of fluid generated by self-propelled motile gyrotactic microorganisms enhances mixing and eliminates nanomaterials buildup in nanofluids. Haq et al. [32] investigated the flow properties of Cross nanomaterials across extended surfaces exposed to Arrhenius activation energy and a magnetic field. Ahmad et al. [33] studied the bioconvection nanofluid flow of gyrotactic motile bacteria with chemical reactions allowed via a porous medium via a stretched surface. Elanchezhian et al. [34] investigated the rate of motile gyrotactic microorganisms in an Oldroyd-B bioconvective nanofluid flow across a stretched surface with a mixed convective and inclination magnetization field. Bhatti et al. [35] conducted a mathematical investigation on the migration of motile swimming microorganisms in non-Newtonian blood-based nanoliquids via an anisotropic limiting artery. Khan et al. [36described the critical rheological properties of Jeffrey's gyrotactic motile microorganism-containing nanofluid over an accelerating formation. Shafiq et al. [37] investigated gyrotactic microorganisms' heat and mass transformation rate in the presence of second-grade nanofluid flow. Kotnurkar et al. [38] investigated the bioconvection swimming of 3rd-grade nanoliquids flowing of motile organisms via Copper-blood nanofluids in porous walls. Muhammad et al. [39] demonstrated the time-dependent movement of magnetization thermophysical Carreau nanofluids transporting motile microorganisms over a rotating wedge through velocity slip and thermal radiation properties. Farooq et al. [40] presented an entropic representation of the 3-D bioconvective flow of Carreau nanoliquids across a cylinder in the presence of magnetic effects. Hosseinzadeh et al. [41] investigated the cross fluid flow of motile microbes and nanomaterials in a three-dimensional stretched cylinder. Some substantial and recent study on bioconvection swimming

microorganism's fluid was explored analytically by various engaging investigators and can be found in Refs. [42–52]. The current research has several applications in nanotechnology [53], electrical and mechanical engineering [54,55], biomedicine, biotechnology [56], medication delivery, cancer therapy [57], food processing [58], and other industries [59,60].

2. Mathematical description

This model deals with the two-dimensional Bioconvectional flow of Cross nanofluid, including swimming motile microorganisms over a cylinder with melting and convective boundary aspects, as illustrated in Fig. 1. The non-linear thermal radiation and thermal conductivity are also considered. The ambient temperature, concentration, and microorganisms are symbolized as T_∞, C_∞ & N_∞. The induced magnetic field and external electric field are neglected owing to the small Reynolds number.

The constitution equation for cross viscosity model is written as [41,61]:

$$\begin{aligned} &\tau = -pI + \mu A_1, \mu = \mu_\infty + (\mu_0 - \mu_\infty)(1/1 + (\Gamma\dot{\gamma})^n) \\ &where \\ &A_1 = grad\ V + (grad\ V)^T, \dot{\gamma} = \sqrt{\frac{1}{2} tr(A_1)^2}, \end{aligned} \tag{1}$$

Here the velocity vector is *V*. let considered the shear rate infinity is zero, hence expression (1) can be written as

$$\mu = (\mu_0)(1\ /\ 1 + (\Gamma\dot{\gamma})^n) \tag{2}$$

For unsteady two dimensional flows, velocity vector, heat, concentration and microorganisms profile are assumed as:

$$V = [v(r,x,t), u(r,x,t)], T = T(r,x,t), C = C(r,x,t). \tag{3}$$

By introducing equation (3) in expressions (1–2), we have governing equations are [62].

$$ru_x + rv_r = 0, \tag{4}$$

$$\begin{aligned} &u_t + uu_x + vu_r = (U_e)_t + U_e\partial_z(U_e) + \frac{\nu}{r}u_r\left[\frac{1}{1+(\Gamma u_r)^n}\right] + \nu\partial_t\left[\frac{u_r}{1+(\Gamma u_r)^n}\right] - \frac{\sigma B^2(t)}{\rho f}(u - U_e) \\ &+ \frac{1}{\rho_f}\left[(1-C_f)\rho_f\beta^* g(T-T_\infty) - (\rho_p - \rho_f)g(C-C_\infty) - (N-N_\infty)g\gamma^{**}(\rho_m - \rho_f)\right], \end{aligned} \tag{5}$$

$$T_t + uT_x + vT_r = \frac{1}{r(\rho c)f}\partial_r(K(T)rT_r) + \frac{1}{r}\partial_r(\alpha rT_r) + \tau\left[D_B C_r T_r + \frac{D_T}{T_\infty}(T_r)^2\right] + \partial_r\left(\frac{16\sigma^*}{3k^*(\rho c)_f}T^3 T_r\right), \tag{6}$$

$$K(T) = k_\infty\left(1 + \in\frac{T - T_\infty}{\Delta T}\right) \tag{7}$$

$$C_t + uC_x + vC_r = \frac{1}{\rho c_p}\partial_r[D(T)C_r] + \frac{D_B}{r}\partial_r(rC_r) + \frac{D_T}{T_\infty}\frac{1}{r}\partial_r(rT_r), \tag{8}$$

$$D(C) = D_\infty\left(1 + \in_1\frac{C - C_\infty}{\Delta C}\right) \tag{9}$$

$$N_t + uN_x + vN_r = D_m(N_{rr}) - \frac{bW_c}{(C_w - C_\infty)}[\partial_r(NC_r)], \tag{10}$$

The boundary conditions are

$$\left.\begin{aligned} &u = u_w(x,t), v = 0, -k_f T_r = -h_f(T - T_w), \\ &D_B C_r + \frac{D_T}{T_\infty}T_r = 0, N = N_w, atr = R, \\ &u \to 0, T \to T_\infty, C \to C_\infty, N \to N_\infty asr \to \infty \end{aligned}\right\}, \tag{11}$$

Also, the melting phenomenon

$$k_f(T_r) = \rho_f\left[\lambda^* + (c_p)_s(T_w - T_0)u\right] \tag{12}$$

The similarity transformations are

$$\left.\begin{array}{l}\psi=(u_w\nu x)^{\frac{1}{2}}Rf(\zeta),\zeta=\dfrac{r^2-R^2}{2R}\left(\dfrac{u_w}{\nu x}\right)^{\frac{1}{2}},\\ \theta(\zeta)=\dfrac{T-T_\infty}{T_w-T_\infty},\varphi(\zeta)=\dfrac{C-C_\infty}{C_w-C_\infty},\chi(\zeta)=\dfrac{N-N_\infty}{N_w-N_\infty}\end{array}\right\},\tag{13}$$

The dimensionless forms of the governing equations are

$$[(1+(1-n)(Wef'')^n)](1+2\alpha\zeta)f'''+2\alpha f''\left[\left\{1+(Wef'')^n\left(1-\frac{n}{2}\right)\right\}\right][1+(Wef'')^n]^2\left[Re\left(ff''+f'^2+1\right)-A\left(f'+\frac{\zeta}{2}ff''\right)-M^2Re(f'-1)\right]$$
$$+\lambda(\theta-Nr\varphi-Nc\chi)=0,\tag{14}$$

Here $\alpha\left(=\frac{1}{R}\sqrt{\frac{\nu l}{U_0}}\right)$ is the curvature parameter, $Nr\left(=\frac{(\rho_p-\rho_f)(C_w-C_\infty)}{(1-C_\infty)(T_w-T_\infty)\beta^*}\right)$ is buoyancy ratio parameter, $Nc\left(=\frac{\gamma^{**}(\rho_m-\rho_f)(N_w-N_\infty)}{(1-C_\infty)(T_w-\widetilde{T}_\infty)\beta}\right)$ is bioconvection Rayleigh number, $A\left(=\frac{c}{a}\right)$ is a time-dependent parameter, $M\left(=\frac{\sigma B_0^2}{\rho C_p}\right)$ is the magnetic parameter, $\lambda\left(=\frac{\beta^*g(1-C_\infty)(T_w-T_\infty)}{\frac{uw}{\nu}}\right)$ is the mixed convection parameter, $We\left(=\frac{u_w r\Gamma^2}{(1-ct)^3\upsilon}\right)$ is Weissenberg number.

$$(1+2\alpha\zeta)(1+\in\theta)\theta''+\in\zeta(\theta')^2+2\alpha\theta'+\Pr f\theta'-\Pr A\frac{\zeta}{2}\theta'+\Pr(1+2\alpha\zeta)(Nb\varphi'\theta'+Nt\theta')+\frac{2}{3N_R}\left[\{1+(\theta_w-1)\theta\}^3(2\theta'\alpha+2\theta''(1+2\alpha\zeta))\right.$$
$$\left.+6\{1+(\theta_w-1)\theta\}^2\right]\times(\theta_w-1)\theta'^2(1+2\alpha\zeta)=0,\tag{15}$$

Here $\Pr\left(=\frac{\nu}{\alpha}\right)$ is the Prandtl number, $Nb\left(=\frac{ED_B(C_w-C_\infty)}{\alpha}\right)$ is the Brownian motion parameter, $Nt\left(=\frac{ED_T(T_w-T_\infty)}{T_\infty\alpha}\right)$ is the thermophoresis parameter, $\theta_w\left(=\frac{T_w}{T_\infty}\right)$ is temperature ratio parameter, $N_R\left(=\frac{kk^*}{4\sigma^*T_\infty^3}\right)$ is radiation parameter.

$$(1+2\alpha\zeta)(1+\in_2\theta)\varphi''+\in_2\varphi'^2+2\alpha\varphi'+PrLef\varphi'+\frac{Nt}{Nb}[(1+2\alpha\zeta)\theta''+2\alpha\theta']-PrLe\frac{\zeta}{2}\varphi'=0,\tag{16}$$

Here $Le\left(=\frac{\alpha}{D_B}\right)$ is Lewis number.

$$(1+2\alpha\zeta)\chi''+2\alpha\chi'+Lbf\chi'-Pe(\varphi''(\chi+\delta_1)+\chi'\varphi')=0,\tag{17}$$

Here $Lb\left(=\frac{\nu}{D_m}\right)$ is bioconvection Lewis number, $Pe\left(=\frac{bW_c}{D_m}\right)$ is Peclet number.

2.1. The dimensionless form of boundary conditions

$$\left.\begin{array}{l}f'(0)=1,f'(\infty)\to0,\\ \theta'(0)=-Bi(1-\theta(0)),\theta(\infty)\to0,\\ Nb\varphi'(0)+Nt\theta'(0)=0,\varphi(\infty)\to0\\ \chi(0)=1,\chi(\infty)\to0\end{array}\right\},\tag{18}$$

Also, the dimensional form of the melting phenomenon

$$\Pr f(0)+Ma\theta'(0)=0,\tag{19}$$

Here $Ma\left(=\frac{c_p(T_\infty-T_w)}{\lambda+c_s(T_w-T_0)}\right)$ is the melting parameter, $Bi\left(=\frac{h_f}{k}\sqrt{\frac{\nu}{c}}\right)$ Biot number.

Here C_f is the skin-friction coefficient, and Nu is the Nusselt number, respectively.

$$\left.C_f=\frac{\tau_{rx}}{\rho_fU^2},Nu=\frac{xq_w}{k(T_w-T)}+q_r\right|_{r=R},\Big\},\tag{20}$$

$$\tau_{rx}=u_0u_r\left[\frac{1}{1+(\Gamma u_r)^n}\right],q_w=-k(T)(T_r)|_{r=R},\tag{21}$$

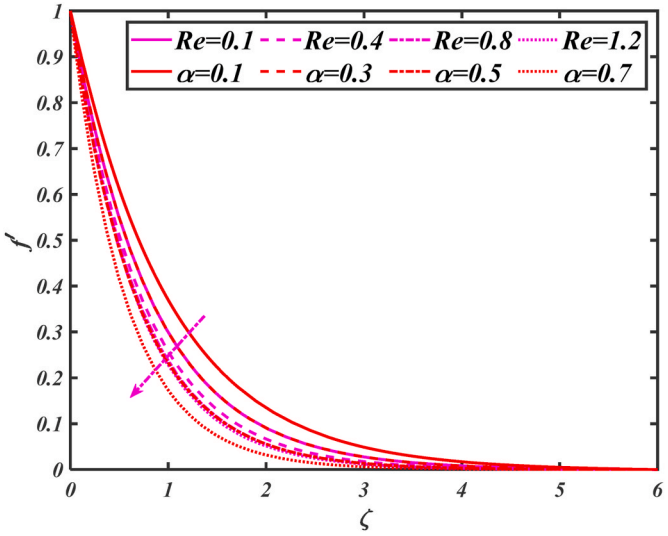

Fig. 2a. Facets of $Re\&\alpha$ versus.$f^{'}$

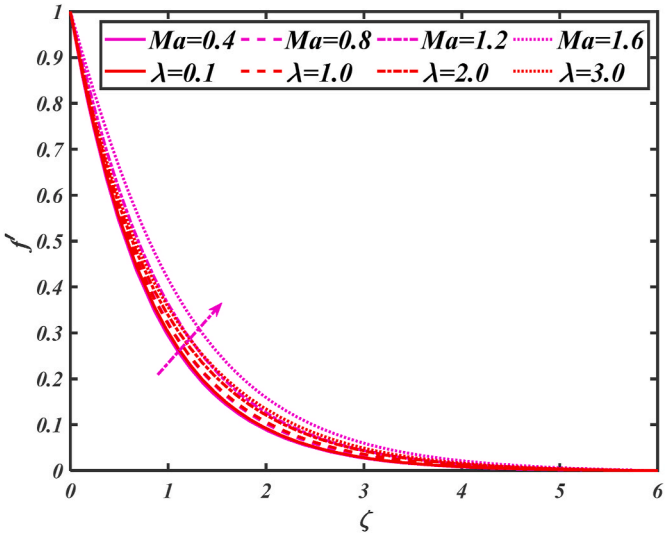

Fig. 2b. Facets of $Ma\&\lambda$ versus.$f^{'}$

$$\left.\begin{aligned} \mathrm{Re}^{\frac{1}{2}}C_f &= f''(0)\left[\frac{1}{1+\{Wef''(0)\}^n}\right], \\ \mathrm{Re}^{\frac{-1}{2}}Nu &= -\theta'(0)\left[1+\frac{4}{2N_R}\left\{[1+(\theta_w-1)\theta(0)]^3\right\}\right], \end{aligned}\right\} \tag{22}$$

Here $\mathrm{Re}=\frac{xu_w}{\nu}$ is the local Reynolds number.

3. Numerical solution

Popular differential expressions (14–17) with boundary constraints (17) are strongly non-linear structures. To tackle these non-linear systems, the shooting scheme known as the bvp4c (Labotto IIIa formula) was employed. The strongly non-linear regulatory equations obtained are presented numerically using bvp4c for MATLAB computational software. Furthermore, the flow controlling parameter specified some constant rage, such as $0.1 \le M \le 0.7, 0.0 \le N_R \le 1.0, 0.1 \le Nc \le 1.5, 0.2 \le Pr \le 5.0, 0.1 \le Nt \le 1.5, 0.1 \le Nb \le 1.2, 0.1 \le Ma \le 1.2, 0.1 \le Bi \le 1.2, 0.1 \le \theta_w \le 1.8, 0.1 \le Pe \le 1.0, 0.2 \le \lambda \le 0.8, 0.1 \le Nr \le 1.2$ are discussed. Before beginning the process, higher differential equations are changed into first-order equations using variables, such as"

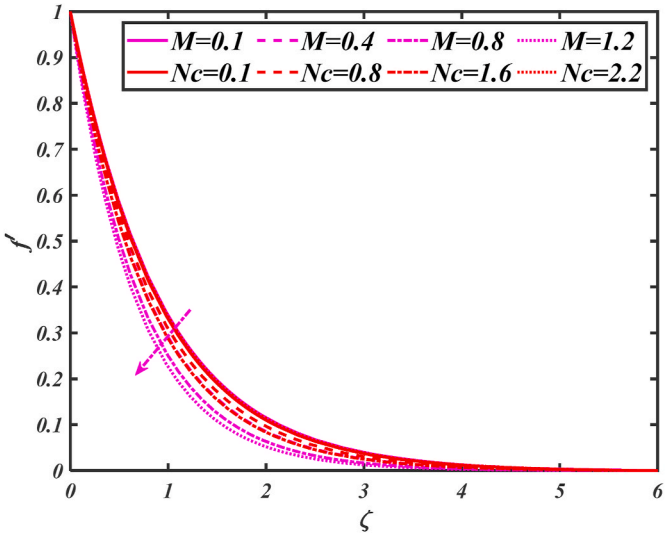

Fig. 2c. Facets of *M&Nc* versus.$f^{'}$

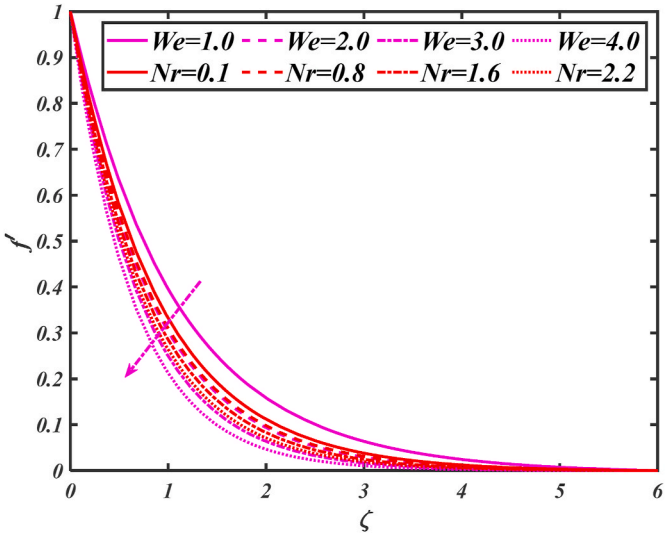

Fig. 2d. Facets of *We&Nr* versus.$f^{'}$

$$\left.\begin{aligned} &f=\boldsymbol{p}_1, \boldsymbol{f}^{'}=\boldsymbol{p}_2, \boldsymbol{f}^{''}=\boldsymbol{p}_3, \boldsymbol{f}^{'''}=\boldsymbol{p}_3^{'},\\ &\theta=\boldsymbol{p}_4, \boldsymbol{\theta}^{'}=\boldsymbol{p}_5, \boldsymbol{\theta}^{''}=\boldsymbol{p}_5^{'},\\ &\varphi=\boldsymbol{p}_6, \varphi^{'}=\boldsymbol{p}_7, \varphi^{''}=\boldsymbol{p}_7^{'},\\ &\chi=\boldsymbol{p}_8, \boldsymbol{\chi}^{'}=\boldsymbol{p}_9, \boldsymbol{\chi}^{''}=\boldsymbol{p}_9^{'}, \end{aligned}\right\}, \tag{23}$$

$$-2\alpha p_3\left[\left\{1+(Wep_3)^n\left(1-\frac{n}{2}\right)\right\}\right][1+(Wep_3)^n]^2\begin{bmatrix} Re\left(p_1p_3+{p_2}^2+1\right)\\ -A\left(p_2+\frac{\zeta}{2}p_1p_3\right)\\ -M^2Re(p_2-1)\end{bmatrix}$$

$$p_3^{'}=\frac{-\lambda(p_4-Nrp_6-Ncp_8)}{[(1+(1-n)(Wep_3)^n)](1+2\alpha\zeta)}, \tag{24}$$

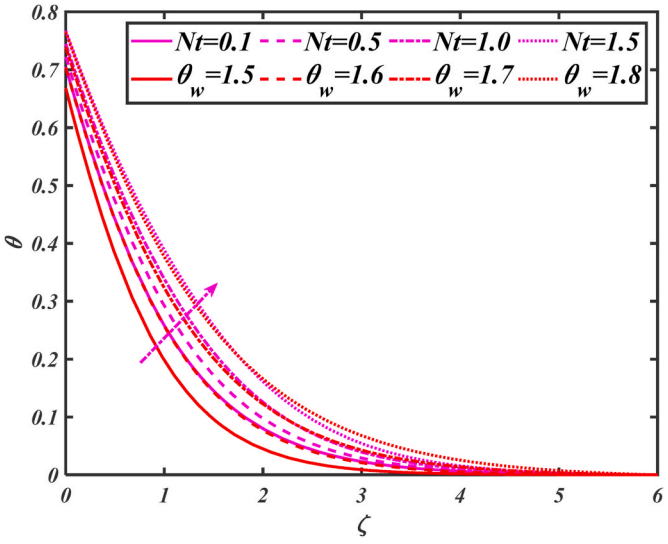

Fig. 3a. Facets of $Nt\&\theta_w$ versus.θ

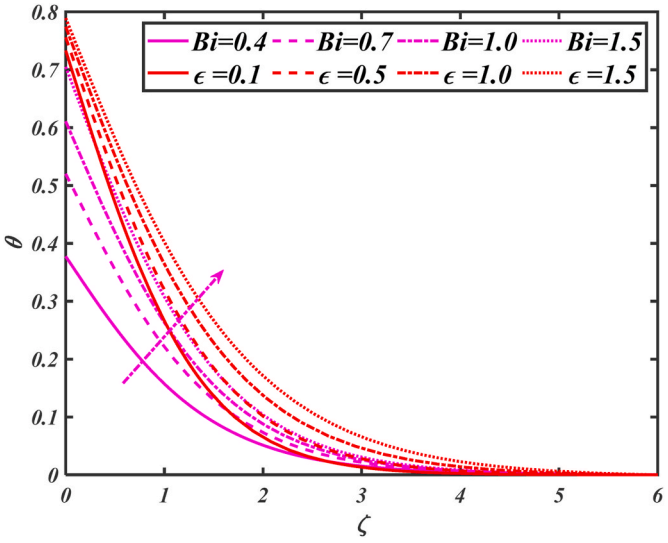

Fig. 3b. Facets of $Bi\& \in$ versus.θ

$$-\in \zeta(p_5)^2 - 2\alpha p_5 - \mathrm{Pr}p_1p_5 + \mathrm{Pr}A\frac{\zeta}{2}p_5 - \mathrm{Pr}(1+2\alpha\zeta)(Nbp_7p_5 + Ntp_5)$$

$$-\frac{2}{3N_R}\left[\{1+(\theta_w-1)p_4\}^3\left(2p_5\alpha + 2p_5'(1+2\alpha\zeta)\right) + 6\{1+(\theta_w-1)p_4\}^2\right]$$

$$p_5' = \frac{\times(\theta_w-1){p_5}^2(1+2\alpha\zeta)}{(1+2\alpha\zeta)(1+\in p_4)}, \tag{25}$$

$$p_7' = \frac{-\in_2{p_7}^2 - 2\alpha p_7 - PrLep_1p_7 - \frac{Nt}{Nb}\left[(1+2\alpha\zeta)p_5' + 2\alpha p_5\right] + PrLe\frac{\zeta}{2}p_7}{(1+2\alpha\zeta)(1+\in_2 p_4)}, \tag{26}$$

$$p_9' = \frac{-2\alpha p_9 - Lbp_1p_9 + Pe\left(p_7'(p_8+\delta_1) + p_9p_7\right)}{(1+2\alpha\zeta)}, \tag{27}$$

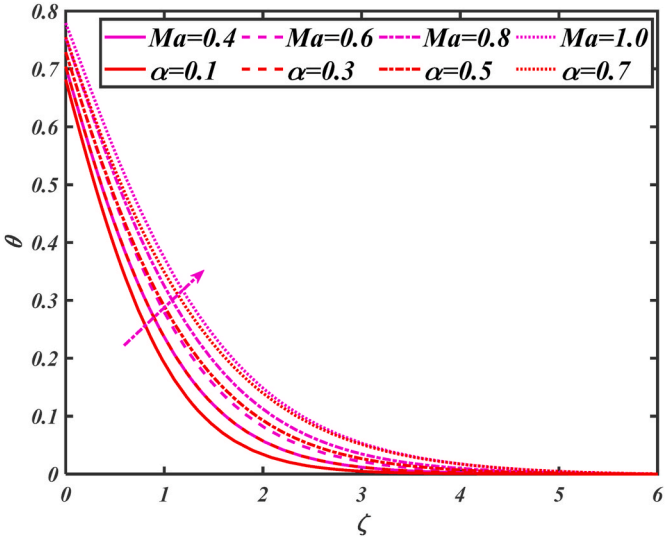

Fig. 3c. Facets of $Ma\&\alpha$ versus.θ

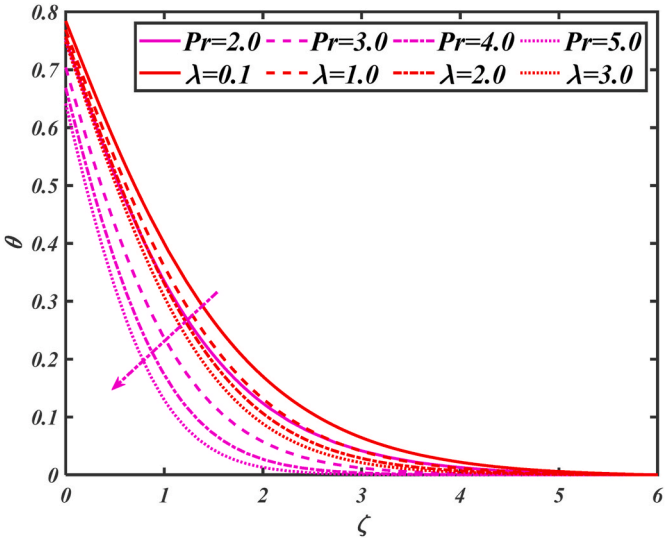

Fig. 3d. Facets of $Pr\&\lambda$ versus.θ

with

$$\left.\begin{array}{l} p_2(0)=1, p_2(\infty)\to 0, \\ p_5(0)=-Bi(1-p_4(0)), p_4(\infty)\to 0, \\ Nbp_7(0)+Ntp_5(0)=0, p_6(\infty)\to 0 \\ p_8(0)=1, p_8(\infty)\to 0 \end{array}\right\}, \tag{28}$$

3.1. Also, with the melting phenomenon

$$\mathrm{Pr}p_1(0)+Map_5(0)=0, \tag{29}$$

4. Results and discussion

In this section, the impact of different flow parameters, including curvature parameter, buoyancy ratio parameter, bioconvection Rayleigh number, time-dependent parameter, magnetic parameter, mixed convection parameter, Prandtl number, Brownian motion

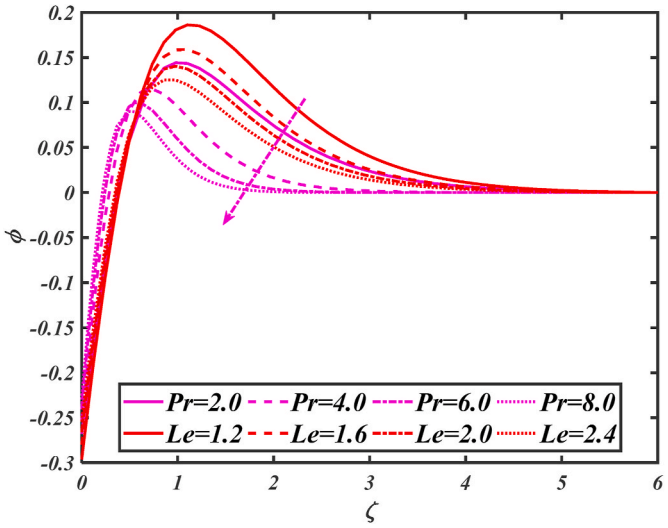

Fig. 4a. Facets of *Pr*&*Le* versus.φ

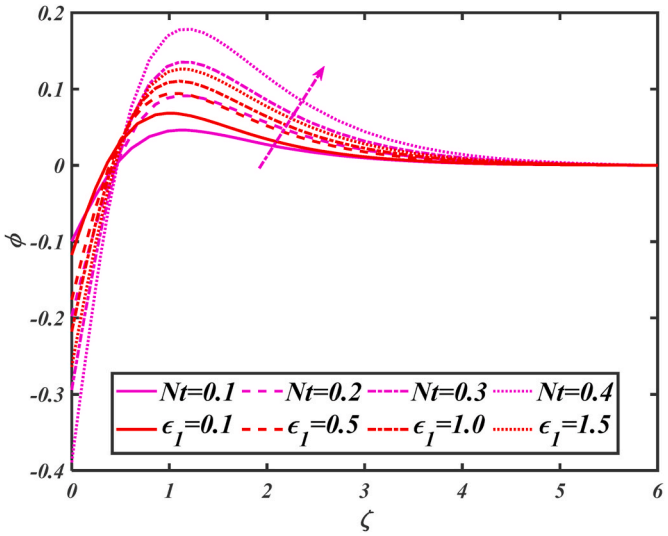

Fig. 4b. Facets of $Nt\&\in_1$ versus.φ

parameter, thermophoresis parameter, temperature ratio parameter, Lewis number, bioconvection Lewis number, Peclet number, melting parameter, and Biot number on each other, have been discussed and are shown in Figs. 2–5. Fig. 2(a) reports the impact of Re and curvature parameter (α) versus the velocity profile$(f^{'})$. The velocity profile is lower for higher Reynolds number and curvature parameter. Fig. 2(b) appearances the influence of the velocity field for various values of melting parameter $(Ma)$and mixed convection parameter(λ). It is comprehended that velocity field upsurges for enhanced variation of both melting parameter parameters and mixed convection parameters. Fig. 2(c) represents the influence of the velocity field on various values of the magnetic parameter (M) and bioconvection Rayleigh number(Nc). As a result, the velocity field decreased for increment in both magnetic parameter and bioconvection Rayleigh number. Fig. 2(d) appearances the influence of the velocity field on different values of the Weissenberg number and buoyancy ratio parameter. As illustrated, the velocity field decline with an increase in the Weissenberg number and buoyancy ratio parameter values. Fig. 3(a) illustrates the effect of the thermophoresis parameter and temperature ratio parameter on the temperature field. It has been witnessed that an enhancement in the thermophoresis parameter and temperature ratio parameter increases the temperature distribution. Fig. 3(b) exhibited the significant features of the Biot number and thermal conductivity on the fluid temperature. As is evident, the temperature distribution (θ) enhances by uprising the magnitude of Biot number and thermal conductivity. The temperature distribution concerning the melting parameter and the curvature parameter is displayed in Fig. 3(c). From these curves, it is noticed that enhancing the melting parameter and curvature parameter augments the temperature distribution.

The efficacy of the temperature field on the Prandtl number and mixed convection parameter (λ) is revealed in Fig. 3(d). From this

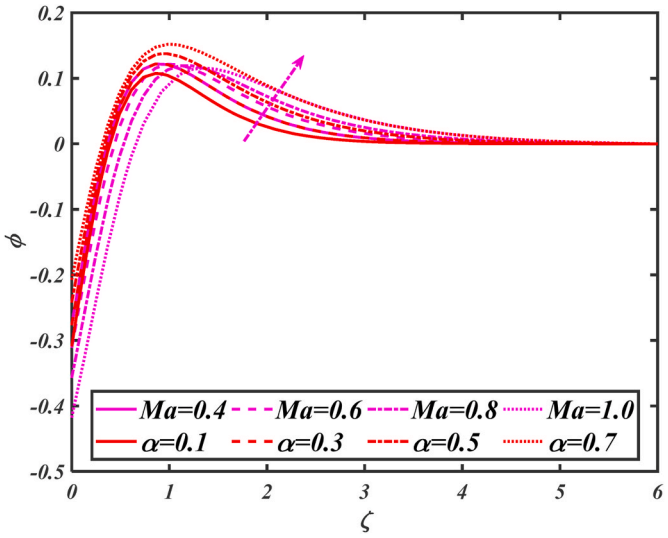

Fig. 4c. Facets of *Ma*&α versus.φ

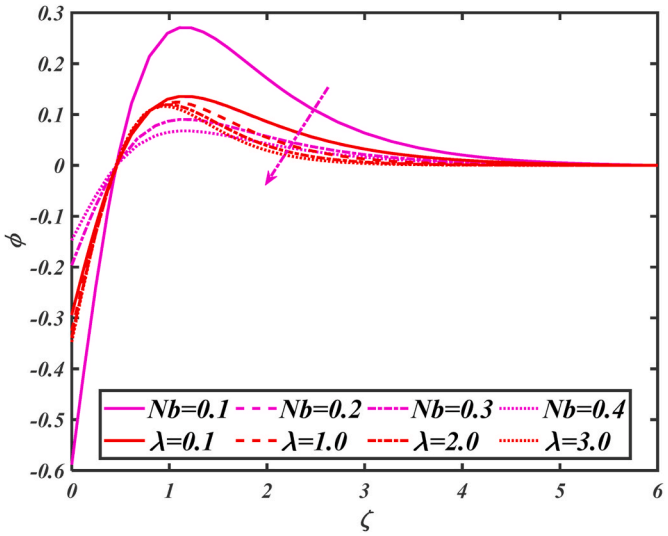

Fig. 4d. Facets of *Nb*&λ versus.φ

figure, it is turned out that the temperature of fluid declines for higher values of (Pr) and λ. Fig. 4(a) demonstrated the influence of the concentration field on the Prandtl number and the Lewis number. Here, it can be noticed that the concentration of nanoparticles reduced with an enormous variety of both parameters, namely Prandtl number and Lewis number. Fig. 4(b) depicted the result of concentration nanoparticles profile on thermophoresis parameter and concentration conductivity($\in_1$). As manifested, nanoparticles' concentration can be improved by growing the variety of thermophoresis parameter and concentration conductivity. Fig. 4(c) indicates the consequence of melting parameter and curvature parameter versus volumetric concentration of nanoparticles. From the observation, it can be noticed that the concentration of nanoparticles is enhanced for higher values of melting parameter and curvature parameter. Features of concentration profile over Brownian motion parameter and mixed convection parameter are plotted in Fig. 4 (d). As an increase in the values of the Brownian motion parameter, the volumetric concentration profile declines. Furthermore, the mixed convection parameter causes a reduction in the volumetric concentration nanoparticle field. The influence of Peclet number and bioconvection Lewis number on the concentration of microorganisms (χ) is displayed in Fig. 5(a). As increment in the value Peclet number and bioconvection Lewis number, the gyrotactic motile microorganism density reduced. Fig. 5(b) represents the nature of the curvature parameter and melting parameter via the microorganism field. As revealed, the microorganism's field enriches the accumulated values of the melting parameter. From this picture, it can be noted that the microorganism's field rises for a more significant curvature parameter (α).

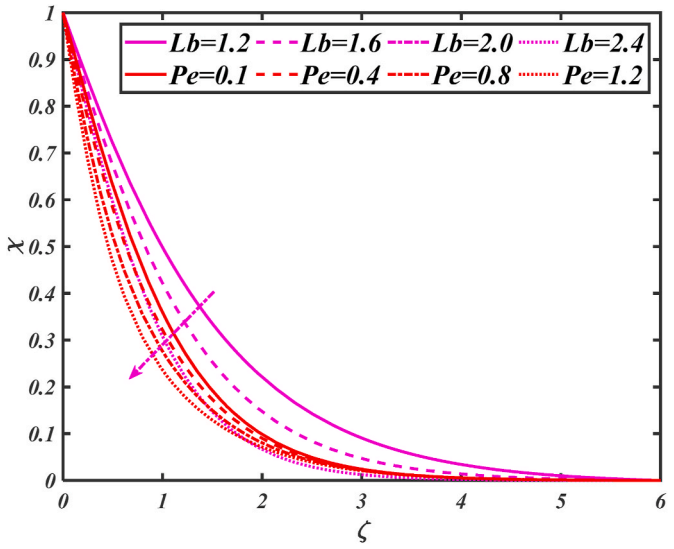

Fig. 5a. Facets of *Lb&Pe* versus.χ

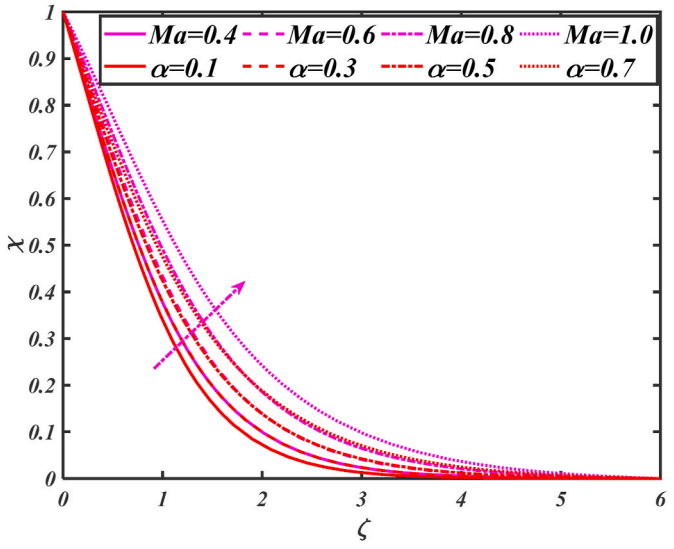

Fig. 5b. Facets of *Ma&α* versus.χ

4.1. Tabular results and discussion

In this portion, the numerical solution of deferent parameters against $-f''(0)$ $-\theta'(0)$, $-\varphi'(0)$ and $-\chi'(0)$ are investigated in Tables 1–4. Table 1 is explored the trend of $-f''(0)$ via various physical parameters. The local skin friction coefficient $-f''(0)$ augments via increasing the *M*a, α, and λ. As enhancement in the value of *M*, *A*, *Nr*, *Nc* magnetic parameter, time-dependent parameter, buoyancy ratio parameter and bio-convection Rayleigh number respectively the local skin coefficient $-f''(0)$ reduced. Table 2 exhibited the influence of different physical parameters on the local Nusselt number $(-\theta'(0))$. It is scrutinized that local Nusselt number depressed with the improvement of *M* but decrement of *Ma*. Table 3 reveals the variation of local Sherwood number $(\varphi'(0))$ via changing the parameters. This numerical outcome disclosed that $\varphi'(0)$ boomed for Pr, while reducing for *M*. Local microorganism number $(-\chi'(0))$ against physical parameters are depicted in Table 4. The $-\chi'(0)$ values enhanced by *Ma and Pe* values augmentation, while it is vanished by increasing the values of *M*.

7. Concluding remarks

In this research, the impact of non-linear thermal radiation with melting phenomenon on the bioconvective flow of Cross nanofluid

Table 1
Estimation of local skin friction coefficients versus physical parameters.

Flow Parameters							Local Skin Friction Coefficients
M	***λ***	***Nr***	***Nc***	***A***	***α***	***Ma***	$-f''(0)$
0.1	0.2	0.1	0.1	0.3	0.3	0.3	**1.1727**
0.4							**1.2468**
0.8							**1.3318**
0.5	**0.5**	0.1	0.1	0.3	0.3	0.3	**1.2598**
	1.0						**1.2451**
	1.5						**1.2305**
0.	0.2	**0.5**	0.1	0.3	0.3	0.3	**1.2699**
		1.0					**1.2714**
		1.2					**1.2720**
0.5	0.2	0.1	**0.5**	0.3	0.3	0.3	**1.2736**
			1.0				**1.2795**
			1.2				**1.2819**
0.5	0.2	0.1	0.1	**0.4**	0.3	0.3	**1.3127**
				0.8			**1.4770**
				1.2			**1.6272**
0.5	0.2	0.1	0.1	0.5	**0.1**	0.3	**1.0327**
					0.6		**1.6947**
					1.2		**2.7111**
0.5	0.2	0.1	0.1	0.5	0.3	**0.1**	**1.2687**
						0.6	**1.2681**
						1.2	**1.2676**

Table 2
Estimation of local Nusselt number versus physical parameters.

Flow Parameters							Local Nusselt Number
M	***Ma***	***Pr***	***Nb***	***Nt***	***Rd***	***α***	$-\theta'(0)$
0.1	0.3	3.0	0.2	0.3	0.5	0.3	**0.6998**
0.4							**0.6928**
0.8							**0.6845**
0.5	**0.4**	3.0	0.2	0.3	0.5	0.3	**0.7021**
	0.8						**0.7463**
	1.2						**0.7883**
0.5	0.3	**3.5**	0.2	0.3	0.5	0.3	**0.7197**
		3.8					**0.7354**
		4.2					**0.7545**
0.5	0.3	3.0	**0.1**	0.3	0.5	0.3	**0.6906**
			0.7				**0.6907**
			1.3				**0.7012**
0.5	0.3	3.0	0.2	**0.1**	0.5	0.3	**0.7216**
				0.5			**0.6589**
				1.0			**0.5777**
0.5	0.3	3.0	0.2	0.3	**0.4**	0.3	**0.7110**
					0.8		**0.6376**
					1.2		**0.5807**
0.5	0.3	3.0	0.2	0.3	0.8	**0.1**	**0.7302**
						0.6	**0.6257**
						1.2	**0.5004**

in the presence of thermal conductivity, gyrotactic motile microorganisms and convective Nield boundary through a cylinder was studied. The Brownian motion and thermophoresis effects are used. A review of previous studies demonstrates that effective heat transmission remains at the forefront of this study field. The unique concept of nanofluid is effective in this regard. Furthermore, in earlier studies, typical Newtonian fluids were used as the base fluid. This work's qualitative attributes include bioconvection, melting phenomenon, radiation parameter and the presence of a non-varying magnetic field. The findings can be used to regulate thermal processes in heat exchangers, vehicles, and electronics. The primary outcomes are pointed out below:

- The velocity field declined for the higher values of magnetic and curvature parameters. However, it boosted up as an increment in the melting parameter values.
- The velocity field grew up as mounting values of mixed convection parameter while the decrease as augmented values of Weissenberg number.

Table 3
Estimation of local Sherwood number versus physical parameters.

Flow Parameters						Local Sherwood Number
M	***Le***	***Pr***	***Nb***	***Nt***	***α***	$\varphi'(0)$
0.1	2.0	3.0	0.2	0.3	0.3	**1.0952**
0.4						**1.0393**
0.8						**1.0268**
0.5	**2.5**	3.0	0.2	0.3	0.3	**1.0318**
	3.0					**1.0284**
	3.5					**1.0254**
0.5	2.0	**3.5**	0.2	0.3	0.3	**1.0796**
		3.8				**1.1031**
		4.2				**1.1318**
0.5	2.0	3.0	**0.1**	0.3	0.3	**2.0719**
			0.7			**0.2960**
			1.3			**0.1594**
0.5	2.0	3.0	0.2	**0.1**	0.3	**0.3608**
				0.5		**1.6473**
				1.0		**2.8883**
0.5	2.0	3.0	0.2	0.3	**0.1**	**1.0952**
					0.6	**0.9385**
					1.2	**0.7505**

Table 4
Estimation of local microorganism number versus physical parameters.

Flow Parameters							Local Microorganism Number
M	***Ma***	***Lb***	***Pe***	***λ***	***Nr***	***Nc***	$-\chi'(0)$
0.1	0.3	2.0	0.1	0.2	0.1	0.1	**1.0535**
0.4							**1.0394**
0.8							**1.0225**
0.5	**0.4**	2.0	0.1	0.2	0.1	0.1	**1.0357**
	0.8						**1.0384**
	1.2						**1.0410**
0.5	0.3	**2.2**	0.1	0.2	0.1	0.1	**1.0981**
		2.4					**1.1588**
		2.8					**1.2744**
0.5	0.3	2.0	**0.2**	0.2	0.1	0.1	**1.1229**
			0.4				**1.2995**
			0.8				**1.6556**
0.5	0.3	2.0	0.1	**0.5**	0.1	0.1	**1.0373**
				1.0			**1.0409**
				1.5			**1.0445**
0.5	0.3	2.0	0.1	0.2	**0.5**	0.1	**1.0336**
					1.0		**1.0341**
					1.2		**1.0339**
0.5	0.3	2.0	0.1	0.2	0.1	**0.5**	**1.0338**
						1.0	**1.0322**
						1.5	**1.0315**

- The temperature field increases for Biot number and temperature ratio parameter boost while declining with Prandtl number augmentation.
- The concentration field boosts for melting parameter and thermophoresis parameter enhancement while reduced for mixed convection parameter improvement.
- The microorganism's field is decreased by growing the Peclet number and Bioconvection Lewis number while increasing for higher melting parameter values.

CRedit author statement

Muhammad Imran & Umar Farooq: Software, Conceptualization, Formal analysis, Visualization, Supervision, Validation, Project administration and Writing - Review & Editing. Hassan Waqas: Methodology, Software, Conceptualization, Formal analysis and Writing - Review & Editing. Ali E. Anqi: Resources, Conceptualization, Validation and Writing - Review & Editing. Mohammad Reza Safaei: Conceptualization, Supervision, Project administration and Writing - Review & Editing.

Declaration of competing interest

The authors declare no conflict of interest.

Acknowledgment

The co-author Ali E. Anqi would like to extend his appreciation to the Deanship of Scientific Research at King Khalid University for the support he received through General Research Project under the grant number (R.G.P.2/138/42).

References

[1] M.M. Sarafraz, Z. Tian, I. Tlili, S. Kazi, M. Goodarzi, Thermal evaluation of a heat pipe working with n-pentane-acetone and n-pentane-methanol binary mixtures, J. Therm. Anal. Calorim. 139 (4) (2020) 2435–2445.
[2] M.H. Ahmadi, B. Mohseni-Gharyehsafa, M. Ghazvini, M. Goodarzi, R.D. Jilte, R. Kumar, Comparing various machine learning approaches in modeling the dynamic viscosity of CuO/water nanofluid, J. Therm. Anal. Calorim. 139 (4) (2020) 2585–2599.
[3] S.A. Bagherzadeh, A. D'Orazio, A. Karimipour, M. Goodarzi, Q.V. Bach, A novel sensitivity analysis model of EANN for F-MWCNTs–Fe_3O_4/EG nanofluid thermal conductivity: Outputs predicted analytically instead of numerically to more accuracy and less costs, Phys. Stat. Mech. Appl. 521 (2019) 406–415.
[4] S.O. Giwa, M. Sharifpur, M. Goodarzi, H. Alsulami, J.P. Meyer, Influence of base fluid, temperature, and concentration on the thermophysical properties of hybrid nanofluids of alumina–ferrofluid: experimental data, modeling through enhanced ANN, ANFIS, and curve fitting, J. Therm. Anal. Calorim. 143 (6) (2021) 4149–4167.
[5] M.H. Bahmani, G. Sheikhzadeh, M. Zarringhalam, O.A. Akbari, A.A. Alrashed, G.A. Shabani, M. Goodarzi, Investigation of turbulent heat transfer and nanofluid flow in a double pipe heat exchanger, Adv. Powder Technol. 29 (2) (2018) 273–282.
[6] S.A. Bagherzadeh, E. Jalali, M.M. Sarafraz, O.A. Akbari, A. Karimipour, M. Goodarzi, Q.V. Bach, Effects of magnetic field on micro cross jet injection of dispersed nanoparticles in a microchannel, Int. J. Numer. Methods Heat Fluid Flow 30 (5) (2019) 2683–2704, https://doi.org/10.1108/HFF-02-2019-0150.
[7] M. Bahiraei, M. Jamshidmofid, M. Goodarzi, Efficacy of a hybrid nanofluid in a new microchannel heat sink equipped with both secondary channels and ribs, J. Mol. Liq. 273 (2019) 88–98.
[8] S.U.S. Choi (Ed.), Enhancing Thermal Conductivity of Fluids with Nanoparticles, vol. 231, ASME Publications-Fed, 1995, pp. 99–106.
[9] J. Buongiorno, Convective transport in nanofluids, J. Heat Tran. 28 (2006) 240–250.
[10] K. Venkatadri, S. Abdul Gaffar, P. Rajarajeswari, V.R. Prasad, B.O. Anwar, K.B.M. Hidayathulla, Melting heat transfer analysis of electrically conducting nanofluid flow over an exponentially shrinking/stretching porous sheet with radiative heat flux under a magnetic field, Heat Transfer (2020), https://doi.org/10.1002/htj.21827.
[11] H. Mondal, S. Bharti, Spectral Quasi-linearization for MHD nanofluid stagnation boundary layer flow due to a stretching/shrinking surface, Journal of Applied and Computational Mechanics 6 (4) (2020) 1058–1068.
[12] Z. Ying, B. He, L. Su, Y. Kuang, D. He, C. Lin, Convective heat transfer of molten salt-based nanofluid in a receiver tube with non-uniform heat flux, Appl. Therm. Eng. 181 (2020), 115922.
[13] N.A. Zainal, R. Nazar, K. Naganthran, I. Pop, Stability analysis of MHD hybrid nanofluid flow over a stretching/shrinking sheet with quadratic velocity, Alexandria Engineering Journal (2020), https://doi.org/10.1016/j.aej.2020.10.020.
[14] M.R. Eid, M.A. Nafe, Thermal Conductivity Variation and Heat Generation Effects on Magneto-Hybrid Nanofluid Flow in a Porous Medium with Slip Condition. Waves in Random and Complex Media, 2020, pp. 1–25.
[15] H. Eshgarf, R. Kalbasi, A. Maleki, M.S. Shadloo, A review on the properties, preparation, models and stability of hybrid nanofluids to optimize energy consumption, J. Therm. Anal. Calorim. (2020) 1–25.
[16] N. Khan, M.S. Hashmi, S.U. Khan, F. Chaudhry, I. Tlili, M.S. Shadloo, Effects of homogeneous and heterogeneous chemical features on Oldroyd-B fluid flow between stretching disks with velocity and temperature boundary assumptions, Math. Probl Eng. (2020), https://doi.org/10.1155/2020/5284906.
[17] I. Tlili, M. Rabeti, M.S. Shadloo, Z. Abdelmalek, Forced convection heat transfer of nanofluids from a horizontal plate with convective boundary condition and a line heat source embedded in porous media, J. Therm. Anal. Calorim. (2020) 1–14.
[18] F.S. Al-Mubaddel, U. Farooq, K. Al-Khaled, S. Hussain, S.U. Khan, M.O. Aijaz, H. Waqas, Double stratified analysis for bioconvection radiative flow of Sisko nanofluid with generalized heat/mass fluxes, Phys. Scripta 96 (5) (2021), 055004.
[19] H. Waqas, U. Farooq, R. Naseem, S. Hussain, M. Alghamdi, Impact of MHD radiative flow of hybrid nanofluid over a rotating disk, Case Studies in Thermal Engineering 26 (2021), 101015.
[20] H. Eshgarf, R. Kalbasi, A. Maleki, M.S. Shadloo, A review on the properties, preparation, models and stability of hybrid nanofluids to optimize energy consumption, J. Therm. Anal. Calorim. (2020) 1–25.
[21] M. Imran, U. Farooq, T. Muhammad, S.U. Khan, H. Waqas, Bioconvection transport of Carreau nanofluid with magnetic dipole and nonlinear thermal radiation, Case Stud. Ther. Eng. (2021) 101129, https://doi.org/10.1016/j.csite.2021.101129.
[22] I. Tlili, M. Rabeti, M.S. Shadloo, Z. Abdelmalek, Forced convection heat transfer of nanofluids from a horizontal plate with convective boundary condition and a line heat source embedded in porous media, J. Therm. Anal. Calorim. (2020) 1–14.
[23] M.H.A. Kamal, A. Ali, S. Shafie, N.A. Rawi, M.R. Ilias, G-Jitter effect on heat and mass transfer of 3-D stagnation point nanofluid flow with heat generation, Ain Shams Engineering Journal (2020), https://doi.org/10.1016/j.asej.2020.03.008.
[24] N.S. Anuar, N. Bachok, N.M. Arifin, H. Rosali, Numerical solution of stagnation point flow and heat transfer over a non-linear stretching/shrinking sheet in hybrid nanofluid: stability analysis, Journal of Advanced Research in Fluid Mechanics and Thermal Sciences 76 (2) (2020) 85–98.
[25] R. Rizwana, A. Hussain, S. Nadeem, Slip Effects on Unsteady Oblique Stagnation Point Flow of Nanofluid in a View of Inclined Magnetic Field, Mathematical Problems in Engineering, 2020.
[26] S.S. Giri, K. Das, P.K. Kundu, Influence of nanoparticle diameter and interfacial layer on magnetohydrodynamic nanofluid flow with melting heat transfer inside rotating channel, Math. Methods Appl. Sci. (2020), https://doi.org/10.1016/j.asej.2020.03.008.
[27] R.P. Sharma, N. Acharya, K. Das, On the Impact of Variable Thickness and Melting Transfer of Heat on Magnetohydrodynamics Nanofluid Flow Past a Slandering Stretching Sheet, 2020.
[28] J.R. Platt, Bioconvection patterns' in cultures of free swimming organisms, Science 133 (1961) 1766–1767.
[29] A.V. Kuznetsov, The onset of nanofluid bioconvection in a suspension containing both nanoparticles and gyrotactic microorganisms, Int. Commun. Heat Mass Tran. 37 (2010) 1421–1425.
[30] A.V. Kuznetsov, Nanofluid bioconvection in water-based suspensions containing nanoparticles and oxytactic microorganisms: oscillatory instability, Nanoscale Res. Lett. 6 (2011) 100.
[31] A.V. Kuznetsov, Non-oscillatory and oscillatory nanofluid bio-thermal convection in a horizontal layer of finite depth, Eur. J. Mech. B Fluid 30 (2010) 156–165.
[32] F. Haq, M. Saleem, M. Ur Rahman, Investigation of natural bio-convective flow of Cross nanofluid containing gyrotactic microorganisms subject to activation energy and magnetic field, Phys. Scripta 95 (10) (2020), 105219.
[33] S. Ahmad, M. Ashraf, K. Ali, Nanofluid flow comprising gyrotactic microorganisms through a porous medium, J. Appl. Fluid Mech. 13 (5) (2020).

[34] E. Elanchezhian, R. Nirmalkumar, M. Balamurugan, K. Mohana, K.M. Prabu, A. Viloria, Heat and mass transmission of an Oldroyd-B nanofluid flow through a stratified medium with swimming of motile gyrotactic microorganisms and nanoparticles, J. Therm. Anal. Calorim. 141 (2020) 2613–2623, https://doi.org/10.1007/s10973-020-09847-w.
[35] M.M. Bhatti, M. Marin, A. Zeeshan, R. Ellahi, S.I. Abdelsalam, Swimming of motile gyrotactic microorganisms and nanoparticles in blood flow through anisotropically tapered arteries, Frontiers in Physics 8 (2020) 95.
[36] S.U. Khan, I. Tlili, Significance of activation energy and effective Prandtl number in accelerated flow of Jeffrey nanoparticles with gyrotactic microorganisms, J. Energy Resour. Technol. 142 (11) (2020).
[37] A. Shafiq, G. Rasool, C.M. Khalique, S. Aslam, Second grade bioconvective nanofluid flow with buoyancy effect and chemical reaction, Symmetry 12 (4) (2020) 621.
[38] A.S. Kotnurkar, D.C. Katagi, Bioconvective Peristaltic Flow of a Third-Grade Nanofluid Embodying Gyrotactic Microorganisms in the Presence of Cu-Blood Nanoparticles with Permeable Walls. Multidiscipline Modeling in Materials and Structures, 2020.
[39] T. Muhammad, S.Z. Alamri, H. Waqas, D. Habib, R. Ellahi, Bioconvection flow of magnetized Carreau nanofluid under the influence of slip over a wedge with motile microorganisms, J. Therm. Anal. Calorim. (2020) 1–13.
[40] U. Farooq, H. Waqas, M.I. Khan, S.U. Khan, Y.M. Chu, S. Kadry, Thermally radioactive bioconvection flow of Carreau nanofluid with modified Cattaneo-Christov expressions and exponential space-based heat source, Alexandria Engineering Journal 60 (3) (2021) 3073–3086.
[41] K. Hosseinzadeh, S. Roghani, A.R. Mogharrebi, A. Asadi, M. Waqas, D.D. Ganji, Investigation of cross-fluid flow containing motile gyrotactic microorganisms and nanoparticles over a three-dimensional cylinder, Alexandria Engineering Journal (2020), https://doi.org/10.1016/j.aej.2020.04.037.
[42] Y. Li, H. Waqas, M. Imran, U. Farooq, F. Mallawi, I. Tlili, A numerical exploration of modified second-grade nanofluid with motile microorganisms, thermal radiation, and Wu's slip, Symmetry 12 (3) (2020) 393.
[43] H. Waqas, U. Farooq, Z. Shah, P. Kumam, M. Shutaywi, Second-order slip effect on bio-convectional viscoelastic nanofluid flow through a stretching cylinder with swimming microorganisms and melting phenomenon, Sci. Rep. 11 (1) (2021) 1–16.
[44] H. Waqas, U. Farooq, S.U. Khan, M.I. Khan, Assessment of bioconvection in magnetized Sutterby nanofluid configured by a rotating disk: a numerical approach, Mod. Phys. Lett. B (2020), https://doi.org/10.1142/S021798492150202X.
[45] H. Waqas, S.U. Khan, M.M. Bhatti, M. Imran, Significance of bioconvection in chemical reactive flow of magnetized Carreau–Yasuda nanofluid with thermal radiation and second-order slip, J. Therm. Anal. Calorim. (2020) 1–14.
[46] S.U. Khan, H. Waqas, T. Muhammad, M. Imran, S. Aly, Simultaneous effects of bioconvection and velocity slip in three-dimensional flow of Eyring-Powell nanofluid with Arrhenius activation energy and binary chemical reaction, Int. Commun. Heat Mass Tran. 117 (2020), 104738.
[47] H. Waqas, U. Farooq, S.A. Khan, H.M. Alshehri, M. Goodarzi, Numerical analysis of dual variable of conductivity in bioconvection flow of Carreau–Yasuda nanofluid containing gyrotactic motile microorganisms over a porous medium, J. Therm. Anal. Calorim. (2021) 1–12, https://doi.org/10.1007/s10973-021-10859-3.
[48] T.A. Yusuf, F. Mabood, B.C. Prasannakumara, I.E. Sarris, Magneto-bioconvection flow of williamson nanofluid over an inclined plate with gyrotactic microorganisms and entropy generation, Fluid 6 (3) (2021) 109.
[49] R.V. Kumar, R.P. Gowda, R.N. Kumar, M. Radhika, B.C. Prasannakumara, Two-phase flow of dusty fluid with suspended hybrid nanoparticles over a stretching cylinder with modified Fourier heat flux, SN Applied Sciences 3 (3) (2021) 1–9.
[50] R.P. Gowda, R.N. Kumar, B.C. Prasannakumara, Two-Phase Darcy-forchheimer flow of dusty hybrid nanofluid with viscous dissipation over a cylinder, Int. J. Algorithm. Comput. Math. 7 (3) (2021) 1–18.
[51] B.J. Gireesha, B.M. Shankaralingappa, B.C. Prasannakumar, B. Nagaraja, MHD flow and melting heat transfer of dusty Casson fluid over a stretching sheet with Cattaneo–Christov heat flux model, Int. J. Ambient Energy (2020) 1–9.
[52] M. Gnaneswara Reddy, R.J. Punith Gowda, R. Naveen Kumar, B.C. Prasannakumara, K. Ganesh Kumar, Analysis of modified Fourier law and melting heat transfer in a flow involving carbon nanotubes, Proc. IME E J. Process Mech. Eng. (2021), https://doi.org/10.1177/09544089211001353, 09544089211001353.
[53] O.A. Akbari, M.R. Safaei, M. Goodarzi, N.S. Akbar, M. Zarringhalam, G.A. Shabani, M. Dahari, A modified two-phase mixture model of nanofluid flow and heat transfer in a 3-D curved microtube, Adv. Powder Technol. 27 (5) (2016) 2175–2185.
[54] S.M. Hosseini, M.R. Safaei, M. Goodarzi, A.A. Alrashed, T.K. Nguyen, New temperature, interfacial shell dependent dimensionless model for thermal conductivity of nanofluids, Int. J. Heat Mass Tran. 114 (2017) 207–210.
[55] Y. Peng, A. Parsian, H. Khodadadi, M. Akbari, K. Ghani, M. Goodarzi, Q.V. Bach, Develop optimal network topology of artificial neural network (AONN) to predict the hybrid nanofluids thermal conductivity according to the empirical data of Al_2O_3–Cu nanoparticles dispersed in ethylene glycol, Phys. Stat. Mech. Appl. 549 (2020), 124015.
[56] M.A. Alazwari, M.R. Safaei, Non-isothermal hydrodynamic characteristics of a nanofluid in a fin-attached rotating tube bundle, Mathematics 9 (10) (2021) 1153.
[57] Z. Li, M.M. Sarafraz, A. Mazinani, T. Hayat, H. Alsulami, M. Goodarzi, Pool boiling heat transfer to CuO-H_2O nanofluid on finned surfaces, Int. J. Heat Mass Tran. 156 (2020), 119780.
[58] Z. Tian, A. Abdollahi, M. Shariati, A. Amindoust, H. Arasteh, A. Karimipour, M. Goodarzi, Q.V. Bach, Turbulent flows in a spiral double-pipe heat exchanger, Int. J. Numer. Methods Heat Fluid Flow 30 (1) (2012) 39–53, https://doi.org/10.1108/HFF-04-2019-0287.
[59] H.R. Goshayeshi, M.R. Safaei, M. Goodarzi, M. Dahari, Particle size and type effects on heat transfer enhancement of Ferro-nanofluids in a pulsating heat pipe, Powder Technol. 301 (2016) 1218–1226.
[60] M.A. Alazwari, M.R. Safaei, Combination effect of baffle arrangement and hybrid nanofluid on thermal performance of a shell and tube heat exchanger using 3-D homogeneous mixture model, Mathematics 9 (8) (2021) 881.
[61] M. Ali, F. Sultan, W.A. Khan, M. Shahzad, H. Arif, Important features of expanding/contracting cylinder for Cross magneto-nanofluid flow, Chaos, Solit. Fractals 133 (2020), 109656.
[62] W.A. Khan, M. Ali, M. Shahzad, F. Sultan, M. Irfan, Z. Asghar, A note on activation energy and magnetic dipole aspects for Cross nanofluid subjected to cylindrical surface, Appl. Nanosci. 10 (8) (2020) 3235–3244.